AD-A106 107 WASHINGTON UNIV ST LOUIS MO SEMICONDUCTOR RESEARCH LAB F/G 20/2
II-IV-V2 CHALCOPYRITES FOR HIGH SPEED DEVICES.(U)
JUL 81 C M WOLFE, G A DAVIS, S J HSIEH AFOSR-79-0096
UNCLASSIFIED 59457-3 AFOSR-TR-81-0646 NL

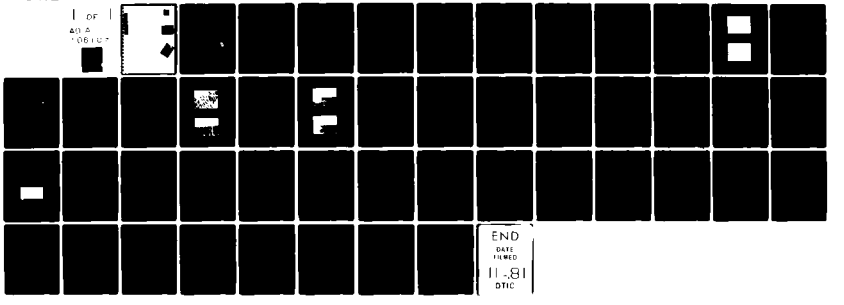

2

LEVEL

nclassified

SECURITY CLASSIFICATION OF THIS PAGE (When Data Entered)

REPORT DOCUMENTATION PAGE		READ INSTRUCTIONS BEFORE COMPLETING FORM
1. REPORT NUMBER AFOSR-TR-81-0646	2. GOVT ACCESSION NO. AD-A106707	3. RECIPIENT'S CATALOG NUMBER
4. TITLE (and Subtitle) II-IV-V_2 Chalcopyrites for High Speed Devices.		5. TYPE OF REPORT & PERIOD COVERED Annual 1 June 80-31 May 81
		6. PERFORMING ORG. REPORT NUMBER 59457-3
7. AUTHOR(s) C.M. Wolfe, G.A. Davis, S. Julie Hsieh		8. CONTRACT OR GRANT NUMBER(s) AFOSR-79-0096
9. PERFORMING ORGANIZATION NAME AND ADDRESS Washington University Box 1127 St. Louis, MO 63130		10. PROGRAM ELEMENT, PROJECT, TASK AREA & WORK UNIT NUMBERS 61102F 2306/BI
11. CONTROLLING OFFICE NAME AND ADDRESS Air Force Office of Scientific Research Building 410 Bolling AFT, DC 20332		12. REPORT DATE 31 July 1981
		13. NUMBER OF PAGES 44
14. MONITORING AGENCY NAME & ADDRESS (if different from Controlling Office)		15. SECURITY CLASS. (of this report) Unclassified
		15a. DECLASSIFICATION/DOWNGRADING SCHEDULE

16. DISTRIBUTION STATEMENT (of this Report)

Approved for public release; distribution unlimited.

17. DISTRIBUTION STATEMENT (of the abstract entered in Block 20, if different from Report)

18. SUPPLEMENTARY NOTES

19. KEY WORDS (Continue on reverse side if necessary and identify by block number)

$Zn_xCd_{1-x}SnP_2$, $ZnGeAs_2$, epitaxial growth, impurities, defects, transport properties, high-speed devices.

20. ABSTRACT (Continue on reverse side if necessary and identify by block number)

An open-tube, sliding-boat, liquid-phase system has been used to grow $Zn_xCd_{1-x}SnP_2$ epitaxially on InP substrates. X-ray diffraction measurements indicate that this alloy grows on {100} substrates with the lattice-matched a-axis in the growth plane and the c-axis in the growth direction. Unintentionally-doped layers have electron concentrations as high as 3×10^{19} cm^{-3} with mobility values of about 2,000 cm^2/V sec. These mobility values are substantially larger than have been obtained in the equivalent III-V materials at similar

DD FORM 1 JAN 73 1473 EDITION OF 1 NOV 65 IS OBSOLETE

Unclassified

concentrations.

Attempts to grow $ZnGeAs_2$ epitaxially on GaAs substrates with a Zn-Ge-$AsCl_3$ and a Zn-$GeCl_4$-Ge-As_4 vapor-phase system have met with little success. Although the first system gives good control over the As flux and the second over Ge, reproducible results have not been achieved in either system. Our experience with these methods, however, indicates that most of the reproducibility problems can be overcome with a Zn-$GeCl_4$-$AsCl_3$ reactor. We are currently investigating this method.

Recent discussions in the literature have pointed out several problems with the conventional theory of heterostructures. We present a general, first-order, nonequilibrium thermodynamic analysis which points out that one problem with conventional theory is that it neglects a generalized thermodynamic force. This force can be associated with the gradient of the effective density-of-states. In heterostructures such gradients cause the charge carriers to move into regions with higher density-of-states, thus increasing the entropy of the system in agreement with the second law of thermodynamics. We also show that if the electrochemical potential is referenced to the infinite vacuum level, then the electron affinity rule must obviously be valid.

Calculations are presented on the I-V characteristics of a space-charge limited diode. If the electrons exhibit inertial motion (are not scattered), then they will quickly reach nonparabolic regions of the conduction band. When this nonparabolicity is taken into account, the current appears ohmic rather than exhibiting a $V^{3/2}$ behavior, as has been previously supposed.

TABLE OF CONTENTS

II-IV-V_2 CHALCOPYRITES FOR HIGH-SPEED DEVICES

1. RESEARCH OBJECTIVES

Because of their lower effective masses, different band structure, and good lattice match to their analog III-V compounds, some of the II-IV-V_2 compounds may be important for heterostructures and high-speed device applications. The objectives of the work reported here are to:

(1) develop techniques for the growth of high-quality epitaxial $Zn_xCd_{1-x}SnP_2$ on InP and GaAs and $ZnGeAs_2$ on GaAs or Ge;

(2) minimize electrically-active defects and residual impurities in these materials to achieve well-controlled doping;

(3) investigate the electrical transport properties of these materials to determine their suitablilty for heterostructures and high-speed device applications; and

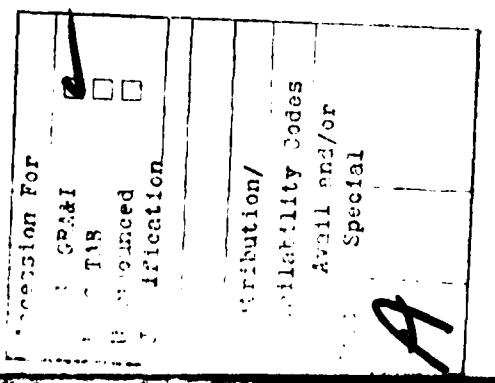

(4) develop the technology required for the fabrication of suitable device structures.

With these results we expect to gain substantial insight into the potential of these II-IV-V_2 chalcopyrites for electronic applications.

2. LIQUID PHASE EPITAXIAL GROWTH OF $Zn_xCd_{1-x}SnP_2$

$CdSnP_2$ is a potentially useful compound semiconductor because it has about half (0.035m) the electron effective mass of its III-IV analog InP with a comparable bandgap (1.17 eV) [1,2]. Previous attempts to grow $CdSnP_2$ epitaxially on InP by LPE have met with limited success due in part to the 0.5% a-to-a mismatch between the two materials [3,4]. The purpose of the work in this section is to develop the technology to produce device quality epitaxial layers to see if the low electron effective mass of this material can be utilized.

2.1 MATERIAL CONSIDERATIONS

A cubic unit cell of the $CdSnP_2$ chalcopyrite structure is compared to two cubic unit cells of the InP sphalerite structure in Figure 1. These crystal structures are similar with the column III element sublattice of the sphalerite structure being replaced by column II element and column IV element sublattices in the chalcopyrite structure. Because of the structure of these sublattices the volume of the chalcopyrite cubic unit cell is approximately twice that of the sphalerite cubic unit cell. The chalcopyrites exhibit uniaxial compression so that two lattice constants are needed to describe the lattice: a and c, where $c/a \leq 2$ for all chalcopyrites. $CdSnP_2$ is an analog of InP since Cd and Sn straddle In on the periodic

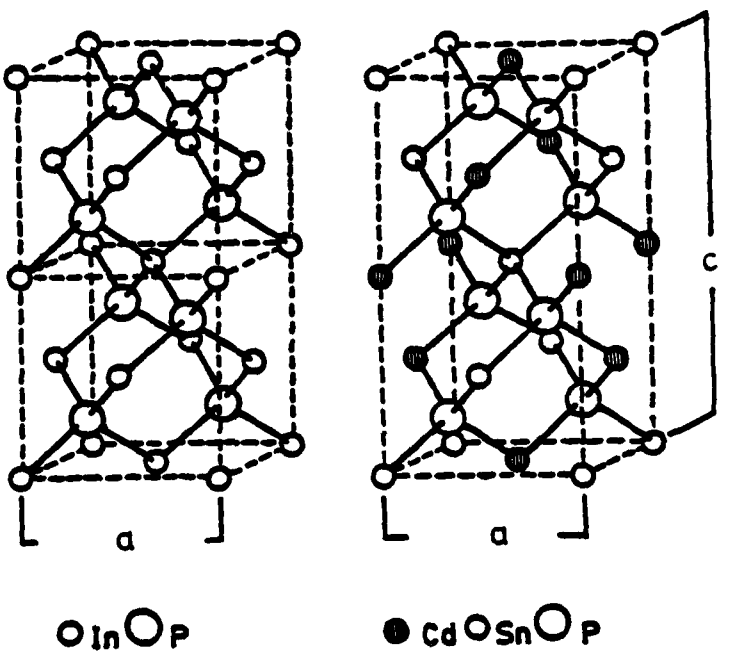

Figure 1 The InP sphalerite and $CdSnP_2$ chalcopyrite lattice structures.

table. Some properties of InP, $CdSnP_2$, and $ZnSnP_2$ are presented in Table 1.

The 0.5% a-to-a mismatch of $CdSnP_2$ on InP has proven to be a serious impediment to the growth of device quality epitaxial layers. A typical $CdSnP_2$ layer grown on InP produced in the early stages of this work is shown in Figure 2. The surface of the grown layer is exceedingly rough and the polycrystalline nature of the layer is revealed in the cross-sectional view. The thin connected layer at the interface is a layer of regrown InP.

To reduce the lattice mismatch in this heterostructure, we decided to grow the lattice matched alloy of $Zn_xCd_{1-x}SnP_2$ although other chalcopyrite alloys could be used, $ZnSnP_2$ was chosen because the lattice matched composition in this case is closer to $CdSnP_2$ than in other possible alloys. Because of the uniaxial compression of the chalcopyrites it is not possible to lattice match both the a and c lattice constants simultaneously. Thus, growth is restricted to {100} oriented InP substrates so that the a lattice constants can be matched at the interface with the c lattice constant extending normal to the growth interface. Such growth is expected from x-ray diffraction measurements of $CdSnP_2$ grown on {100} InP. Assuming Vegard's law, the calculated alloy composition to lattice match InP is $Zn_{0.13}Cd_{0.87}SnP_2$.

Table 1 Physical properties of InP, $CdSnP_2$, and $ZnSnP_2$.

	InP	$CdSnP_2$	$ZnSnP_2$
a(A)	5.8688	5.900	5.651
c(A)	—	11.513	11.302
c/a	—	1.951	2.00
Eg(cv)	1.28	1.17	1.66
M.P.(C)	1070	570	930

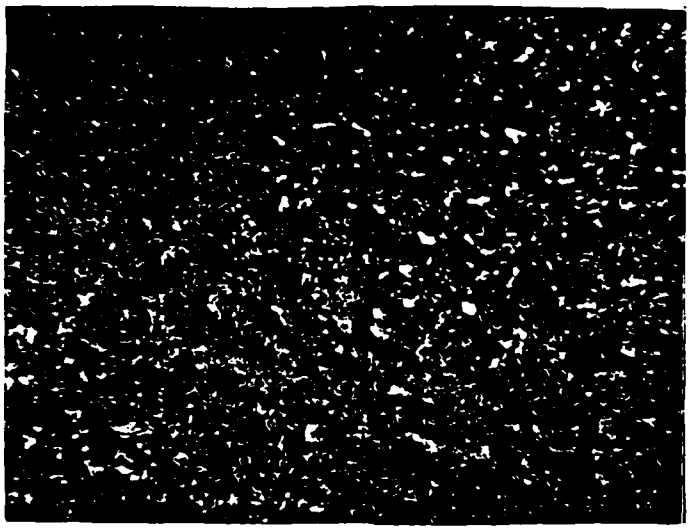

Figure 2 Grown layer of $CdSnP_2$ on InP.

2.2 GROWTH PROCEDURE

The system shown schematically in Figure 3 was used for the epitaxial growth. This system employs a standard LPE graphite boat modified so that the substrate sits in the base with the melt wells extending through the slider. This boat was designed so that growth experiments could be carried out despite the lack of phase diagram information for this system. It also allows us to initiate growth with a saturated solution despite the loss of volatile constituents from the melt during homogenization.

During homogenization the slider is positioned so that its melt wells are aligned with the holes in the top section. In this position the substrate is covered by the slider to reduce the amount of volatile constituents reaching its surface. These contitutents react with the substrate causing severe pitting. Excess source materials, which have been added to the melt, float to the surface to keep the solution saturated as volatile constituents evaporate. Growth is initiated by separating the melt contained in the slider from the rest of the solution. This effectively removes the excess source material before the melt is positioned over the substrate. In this position the growth melt is covered by the top section to reduce depletion due to evaporation.

The growth parameters used in the system for epitaxial growth are presented in Table 2. The source materials used

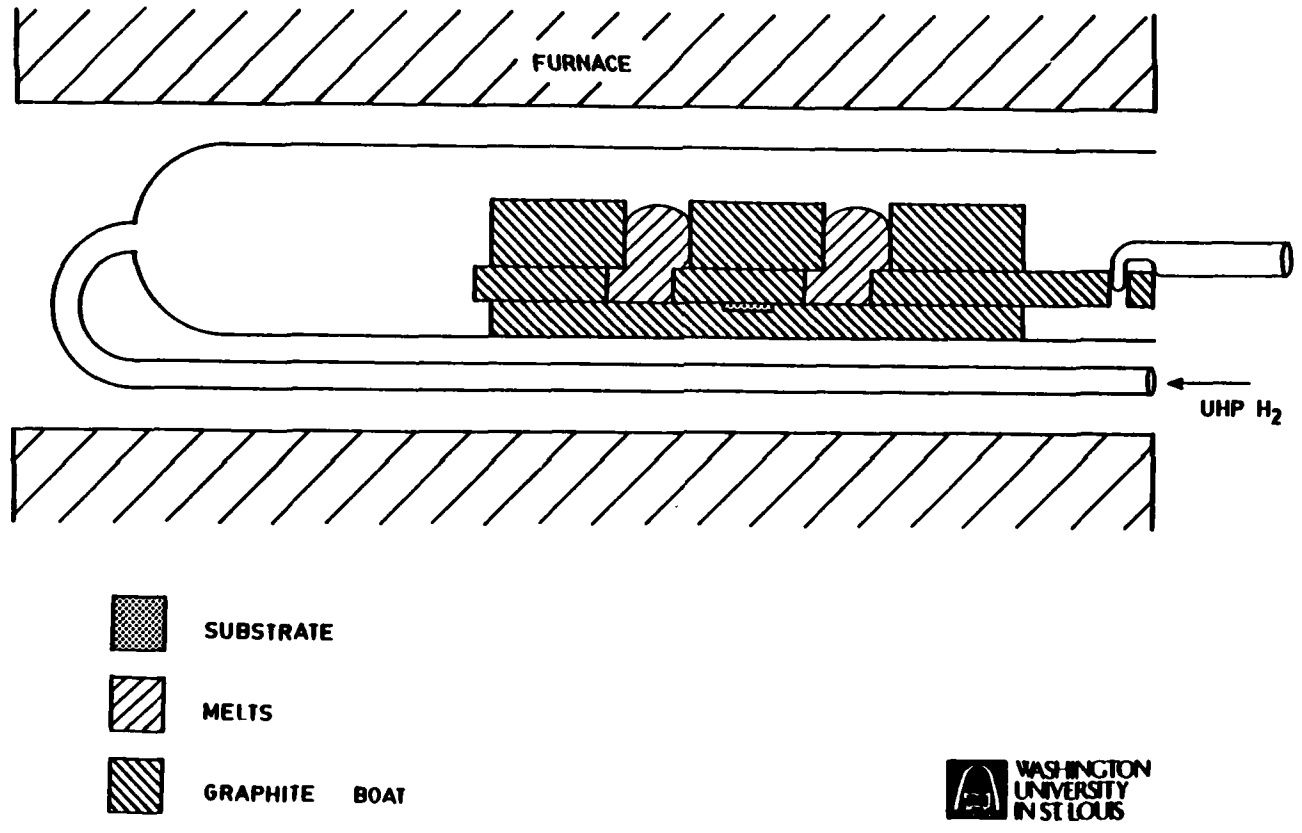

Figure 3 System used for LPE growth of $Zn_xCd_{1-x}SnP_2$.

Table 2 Typical growth parameters for the Zn-Cd-SnP_3-Sn system.

SOURCE MATERIALS: Zn, Cd, SnP_3, Sn

Melt Composition

$CdSnP_2$	19.85	Molar %
$ZnSnP_2$	0.25	Molar %
Sn	77.50	Molar %
P	2.40	Molar %

$ZnSnP_2/CdSnP_2 \simeq 0.0125$

Substrates: {100} Fe Doped InP

Homogenization Temperature: 540°C

Cooling Rate:	5°C/hour
Growth Duration:	10 to 22 hours
in situ Etch:	Pure Sn
Growth Atmosphere:	UHP H_2
Flow Rate:	30 ml/min

are 5Ns purity Zn, Cd, and Sn with SnP_3 used as a source of phosphorus. The SnP_3 was synthesized in a sealed tube system using 5N Sn and red P_4. The melts had an initial equivalent composition of 19.85% $CdSnP_2$, 0.25% $ZnSnP_2$, 2.40% excess P, and 77.50% Sn. This gives a $ZnSnP_2$ to $CdSnP_2$ ratio in the melt of 0.0125 which is about a tenth of the ratio required in the solid to lattice match InP.

A homogenization and initial growth temperature of 540°C was used. For an initial growth temperature of 530°C the growth was often polycrystalline. It should be noted that these temperatures are quite close to the 570°C maximum melting point of $CdSnP_2$. After the growth melt is positioned over the substrate, the furnace is cooled at a linear rate of 5°C/hour. Cooling rates of 10°C/hour produced polycrystalline layers and rates of 4°C/hour produced no growth due to melt depletion by evaporation. Cooling times between 10 and 22 hours were used. A 10 hour cooling time gave 1μm to 2μm of growth, while a 22 hour time gave around 15μm of growth.

In most instances an *in situ* etch of the substrate in pure Sn was made prior to growth. A typical epitaxial layer grown using these parameters is shown in Figure 4. As can be seen from this figure $Zn_xCd_{1-x}SnP_2$ epitaxial layers are much smoother than the $CdSnP_2$ layers grown on InP, although they are still not of device quality. The black regions in the view of the upper surface are etch

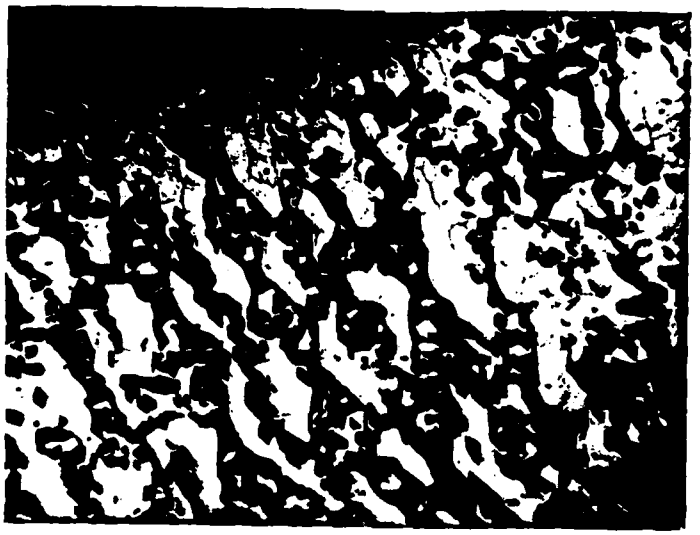

110x

15 µm

Figure 4 Epitaxial layer of $Zn_xCd_{1-x}SnP_2$ grown on {100} InP.

pits which show up as notches in the cross-sectional view. These pits extend to various depths into the epitaxial layers and often extend to the interface.

The sharp dependence of the layer morphology on zinc concentration in the melt is shown in Figure 5. This figure shows two epitaxial layers grown in the same manner except for the zinc concentration in the melts. The layer shown in Figure 5a was grown from a standard melt and that shown in Figure 5b was grown from a melt having a 6% larger mass of zinc. This latter layer is polycrystalline.

2.3 ELECTRICAL MEASUREMENTS

Van der Pauw measurements were obtained for the epitaxial layers with the results shown in Figure 6. All these layers were n type. Most had room temperature calculated carrier concentrations around 10^{18} cm^{-3} and mobilities around 100 cm^2/V sec, similar to layers of $CdSnP_2$ grown on InP. The resistivities were around $3 \times 10^{-2} \Omega$ cm. Notice there are no substantial changes in these values for measurements made at 77 K. One layer had a mobility of 2000 cm^2/V sec with a carrier concentration of 3×10^{19} cm^{-3}. The resistivity of this sample was $1 \times 10^{-4} \Omega$ cm. This sample is of interest because the mobility is about twice that which can be obtained for equivalent III-V compounds at similar carrier concentrations. This sample indicates one potential advantage of the low effective mass II-IV-V_2 chalcopyrites over the III-V sphalerite semiconductors.

(a)

(b)

Figure 5 Epitaxial layers grown from melts of (a) standard composition, and (b) standard composition with a 6% greater Zn mass.

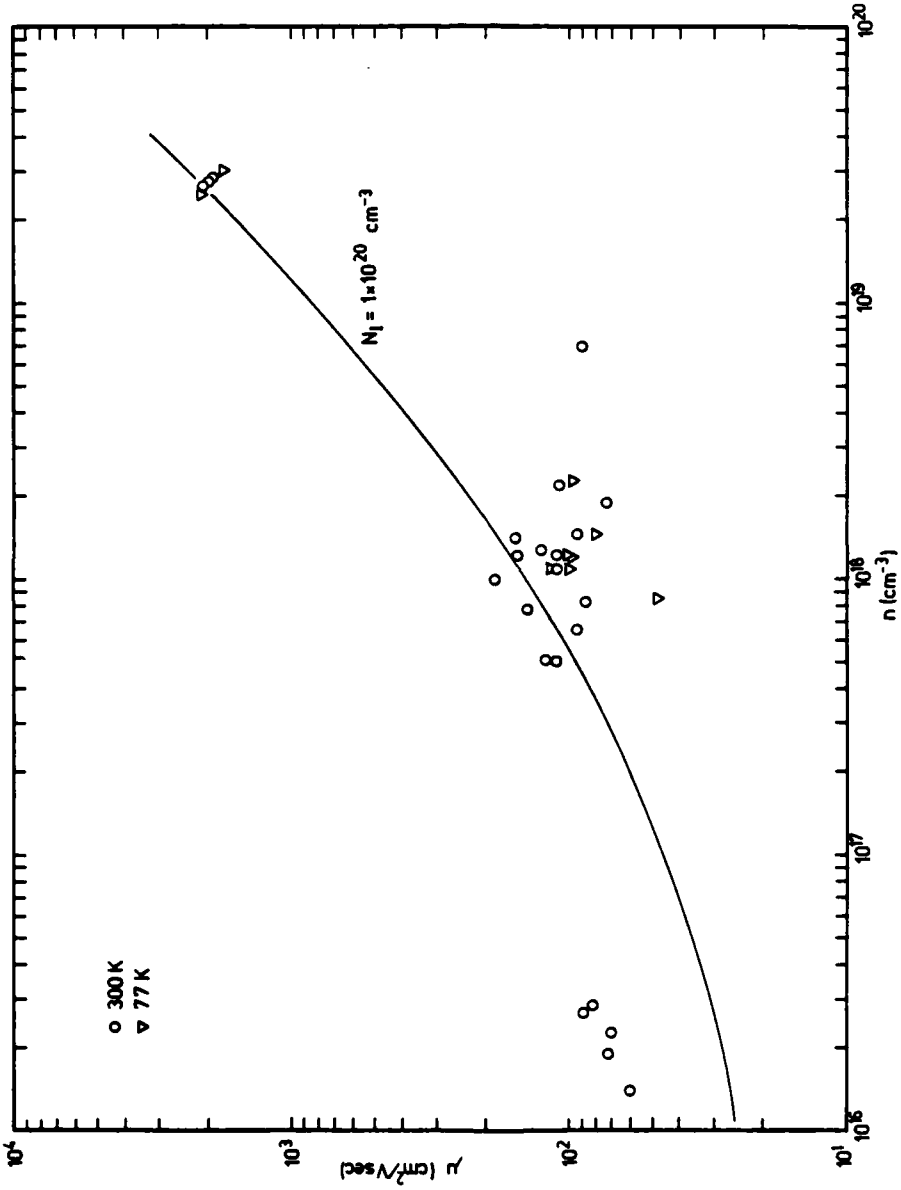

Figure 6 Results of Hall measurements for $Zn_xCd_{1-x}SnP_2$ epitaxial layers.

That is, higher mobilities can be achieved at similar carrier concentrations.

The solid line in Figure 6 shows the theoretical dependence of the mobility on the carrier concentration for scattering from ionized impurities with screening. This curve was calculated from the Brooks-Herring model [5] using degenerate statistics to allow for the high carrier concentrations. The concentration of ionized impurities, N_I, in this model was used as the only adjustable parameter. To fit the high mobility data, a value of $N_I = 1 \times 10^{20} cm^{-3}$ was used. As can be seen, there is reasonable agreement between the experimental data and the theoretical curve. This indicates that the decrease in mobility with decreasing carrier concentration is mostly due to heavy compensation.

Because high conductivity in homogenieties in an epitaxial layer can give anomalously high calculated mobilities [6], further experiments were performed on the high mobility sample to determine whether the mobility value was real. First this sample was cleaved into four pieces and the pieces remeasured. The effects of a conducting inhomogeniety on resistivity and Hall measurements can usually be eliminated in this manner. The mobilities and carrier concentrations of each piece, however, were very close to those of the original sample. This can be seen from the tight grouping of the data in the high concentration region of Figure 6. To further substantiate these data, measurements

of the Hall constant as a function of magnetic field were performed. These results are plotted in Figure 7, where a decrease in the Hall constant with increasing magnetic field is shown. This behavior is typical of homogeneous n-type material. If there had been a conducting inhomogeniety, such as those which give anomalously high calculated mobilities, the Hall constant would have increased with increasing magnetic field. Thus, the mobility and carrier concentration of this epitaxial layer are apparently not due to inhomogeniety effects and appear to be an accurate indication of the high mobility which can be attained in this material.

The high ionized impurity concentration in these samples may be due to loss of volatile constituents from the epitaxial layers during growth. This is supported by the results of high temperature Hall measurements on SiO_2 encapsulated platelets of $CdSnP_2$. These measurements showed a decreasing mobility and increasing carrier concentration with annealing time. Annealing of the layers in a phosphorus or phosphorus and cadmium overpressure should then give increasing mobilities and decreasing carrier concentrations as N_I is reduced. Such experiments are the subject of a future investigation.

2.4 CONCLUSIONS

The method presented for the LPE growth of the lattice matched alloy $Zn_xCd_{1-x}SnP_2$ on InP has yielded epitaxial

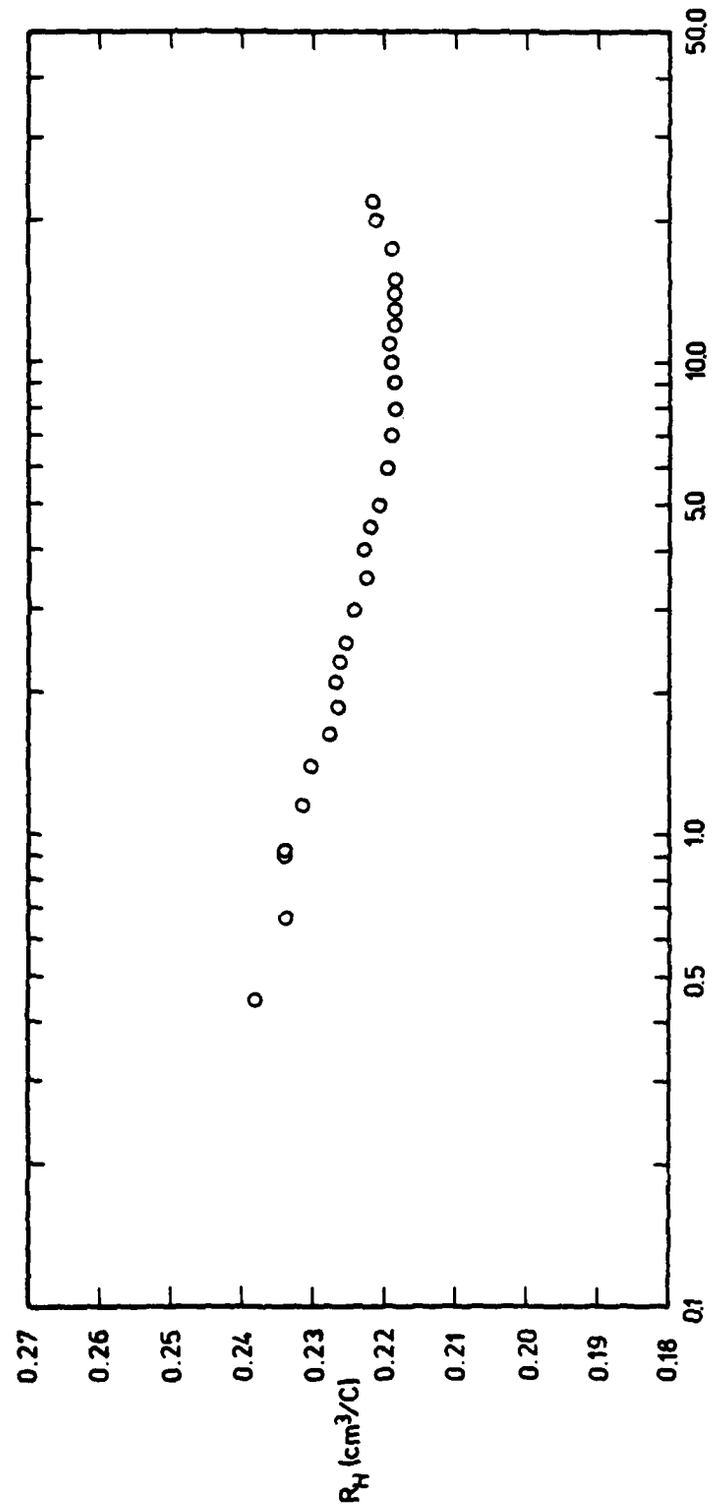

Figure 7 Hall constant as a function of magnetic field for a high mobility sample.

layers substantially better than layers of $CdSnP_2$ on InP. The morphology of these layers, However, is not of device quality. The reasons for this poor morphology may be: (1) zinc depletion from the melt due to its high segregation coefficient; (2) constitutional supercooling; and/or (3) antiphase boundaries due to the additional sublattices of the layer compared to the substrate. We are currently investigating these possibilities.

Van der Pauw measurements on the epitaxial layers have shown that the mobility of this material appears to be substantially higher than can be obtained in equivalent III-V compounds at similar carrier concentrations. Further work needs to be done to substantiate this finding. We plan to perform additional growth experiments as well as annealing experiments to determine if these higher mobility values can be obtained at lower carrier and ionized impurity concentrations.

3. VAPOR PHASE EPITAXIAL GROWTH OF $ZnGeAs_2$

The tetragonal chalcopyrite compound $ZnGeAs_2$ with a bandgap of 1.15eV is a structural and electronic analog of GaAs. If it could be reproducibly prepared in single crystalline form and suitably doped, $ZnGeAs_2$ could be an interesting material for microwave devices. In this section we discuss vapor phase techniques which have been used in an attempt to achieve this purpose.

3.1 GROWTH PROCEDURE

Attempts to synthesize $ZnGeAs_2$ were carried out by employing high purity materials Zn, Ge, As, and $GeCl_4$. The substrates were semi-insulating Cr-doped GaAs. Figure 8 shows the reactor which was used for this purpose. It consists of a silica tube in a furnace with three independently controllable zones. The left hand zone controls the As vapor pressure, the center zone controls the Zn vapor pressure, and the right hand zone is the reaction zone. The $GeCl_4$ is contained in a bubbler held at 0 to 10° C and H_2 is used as the carrier gas. An additional H_2 flow is also provided to flush the reaction tube and to sweep the reactants into the reaction zone.

The GaAs wafers used in the experiments were lapped smooth and etched vigorously in an etch consisting of $5H_2SO_4:1H_2O_2:1H_2O$ to produce a bright, mirror finish.

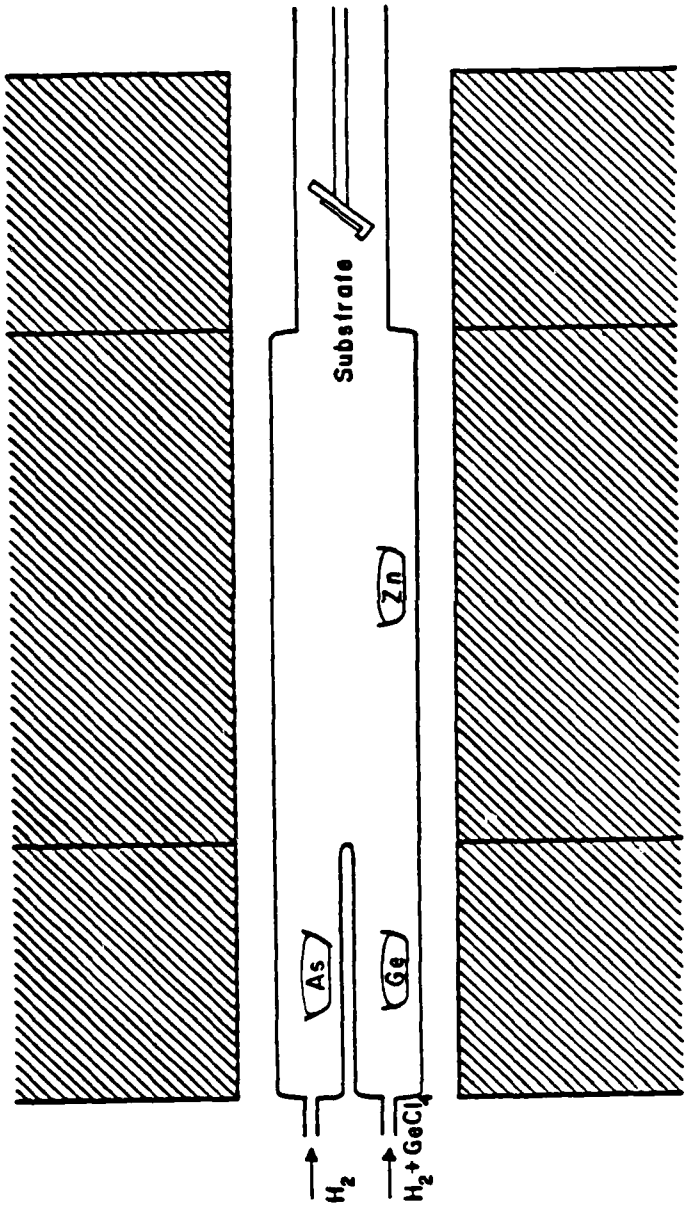

Figure 8 Zn-$GeCl_4$-Ge-As_4

The H_2 flow rate for $GeCl_4$ was 100 ml/min. The additional H_2 flow rate was 100 ml/min.

To try to find the experimental conditions under which $ZnGeAs_2$ could be grown, the Zn and As temperatures were set at 600 and 580° C, respectively. These temperatures provided a large enough flux of these species to essentially flood the reactor zone. With the Ge temperature set at 560° C to produce the disproportionation reaction with $GeCl_4$, the temperatures of the $GeCl_4$ and the reaction zone were systematically varied. Over most of the range of these experiments, little or no growth occurred on the {100} GaAs substrates. With substrate temperatures around 700° C and $GeCl_4$ temperatures in the range from 4 to 10° C, a number of good quality epitaxial layers were obtained. Subsequent analysis, however, indicated that these layers were mostly Ge.

3.2 EXPERIMENTAL RESULTS

Figure 9 shows the upper surface and interface of one of these Ge-GaAs heterostructures. Resistivity and Hall measurements on these Ge epitaxial layers on semi-insulating GaAs substrates indicated very high n-type conductivity. Typical values of electron concentration and mobility were $5 \times 10^{19} cm^{-3}$ and 100 cm^2/V sec, respectively. Some of these n+ Ge layers were also grown on $10^{15} cm^{-3}$ n-type GaAs. The specific contact resistance

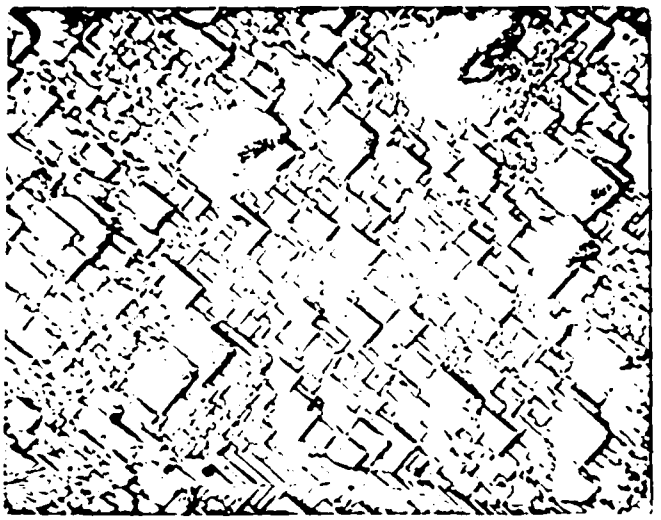

(a) Surface

(b) Interface

Figure 9 Ge-GaAs heterostructure grown in the $GeCl_4$ system

of these n-n+ heterostructures was about $0.1\Omega cm^2$. Although these Ge layers are quite good, we were not able to grow the compound $ZnGeAs_2$ under these conditions.

Since the preparation of the compound appears to be so critically dependent upon the reaction conditions, x-ray diffraction measurements were made to determine the composition of the material deposited at various places in the reactor. Several growth runs were made with different growth parameters. The materials deposited out at the different places of the furnace tube were prepared for diffraction analysis by grinding them into a fine powder and placing them on a flat plate. This plate was then inserted into the specimen holder of the diffractometer. Several diffraction patterns were obtained. The materials were then identified from their diffraction data with the aid of a Hanawalt index and file. Some of these results are shown in Table 3.

Typically, the factors which affected the nature of the deposits most were substrate temperature and reactant ratios. Polycrystalline As was formed downstream at lower temperatures while Ge and Zn_3As_2 were formed at higher temperatures. The Ge/H_2 ratio or Ge input flux variations were achieved by changing the vapor pressure at the $GeCl_4$ source while keeping the total flow constant. The data show a strong Ge growth rate dependence with Ge/H_2 ratio. The choice of reactant vapor pressure ratio, $Zn:GeCl_4:As_4$,

Table 3

An Investigation with X-ray Diffraction

sample	T_{zn} (°C)	T_{GeCl_4} (°C)	T_{As} (°C)	P_{zn} (torr)	P_{GeCl_4} (torr)	P_{As} (torr)	$T_{substrate}$ (°C)	growth composition
1	600	1	580	11.26	24.3	696	350	poly As
2	600	4.1	580	11.26	29.04	696	360	poly As
3	600	4.1	580	11.26	29.04	696	720	10.1μ Ge layer
4	600	10.1	460	11.26	40	21.1	720	18μ Ge layer
5	660	5.3	500	32.01	34.12	65.26	660	Ge and Zn_3As_2 platelets

appears to be important. When the ratio is 1:1:2, large quantities of Zn_3As_2 platelets form together with Ge platelets.

3.3 CONCLUSIONS

The preparation of $ZnGeAs_2$ with the $Zn\text{-}GeCl_4\text{-}Ge\text{-}As_4$ system was found to be much too strongly dependent upon the various growth parameters. When As_4 was transported over the Zn boat, Zn_3As_2 platelets were formed. Apparently, this greatly reduces further transport of Zn or As vapor and results in the depletion of Zn or As in the reaction zone. This appears to be the main problem with this $Zn\text{-}GeCl_4\text{-}Ge\text{-}As_4$ system: it gives excellent control of the Ge flux, but very little control for Zn and As. Previous to this study, we investigated a $Zn\text{-}Ge\text{-}AsCl_3$ reactor system for the synthesis of $ZnGeAs_2$ and found that it produced good As control. For these reasons we are currently attempting to synthesize the compound in a $Zn\text{-}GeCl_4\text{-}AsCl_3$ reactor, which incorporates the best features of the two previous systems without their disadvantages.

This new system is shown in Figure 10. The reactor consists of a 44 mm (OD) quartz tube having separate reactant inlets and a furnace with three independently controllable zones. The flow rates of Zn, $GeCl_4$, and $AsCl_3$ are adjusted by independent carrier gas flowmeters.

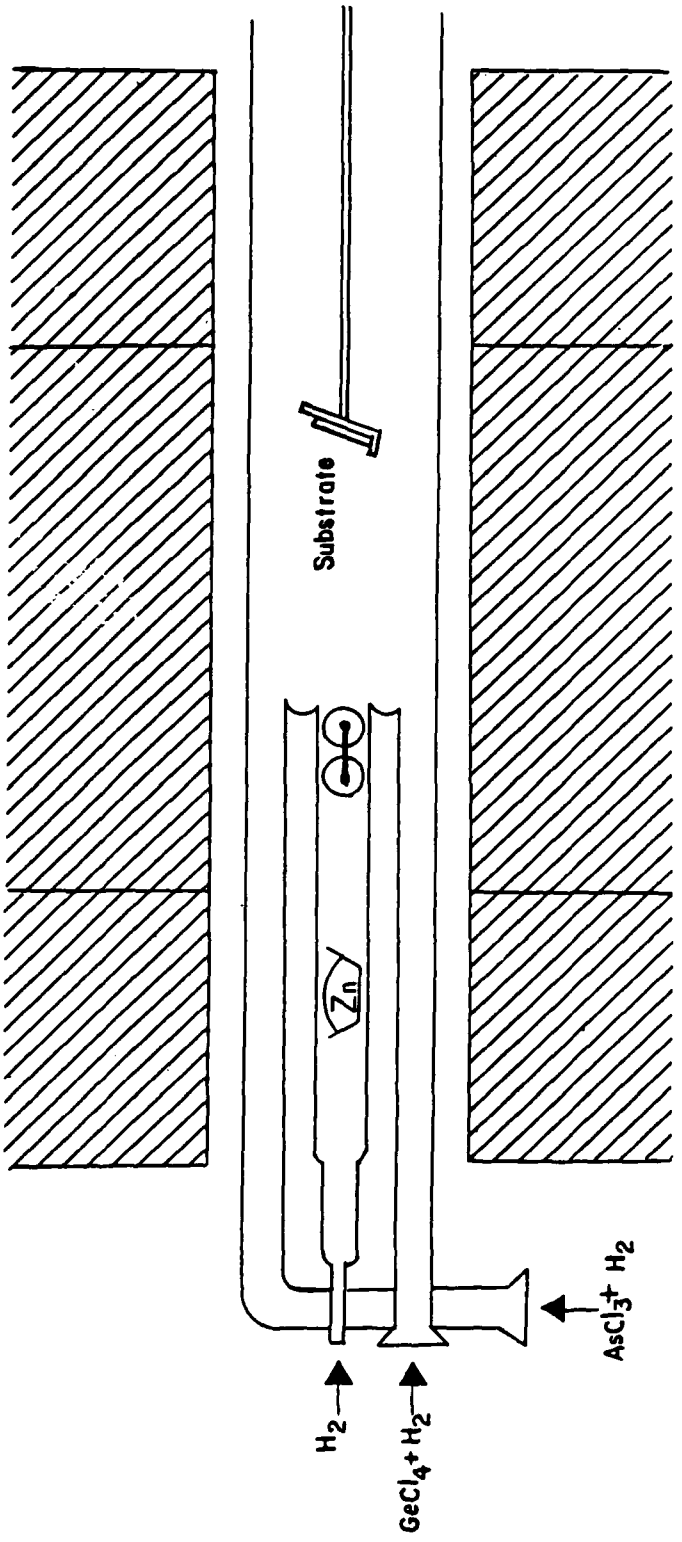

Figure 10 Zn-$GeCl_4$-$AsCl_3$ Reactor System

The left hand zone controls the Zn vapor pressure, while the right hand zone is the reaction zone. A baffle in the Zn chamber is used to isolate the Zn from the As. The $AsCl_3$ and $GeCl_4$ are kept in external bubblers. The primary advantages of this system are: (1) it ensures that the constituents do not react until they reach the reaction zone; (2) it provides better over all control of the three constituents; and (3) it utilizes only one solid source which makes it much simpler to operate than the previous reactor systems.

4. NONEQUILIBRIUM THERMODYNAMICS OF HETEROJUNCTION

The recent interest in heterostructures for lasers, transistor emitters, real-space transfer devices, quantum well lasers, modulation-doped superlattices, and other devices, has prompted a re-examination of basic heterojunction theory. To understand quantitatively the operation of these devices it is necessary to determine how the discontinuity in the energy gaps of a heterostructure is divided between the conduction and valence bands:

$$\Delta\varepsilon_g = \Delta\varepsilon_c + \Delta\varepsilon_v \tag{1}$$

The basic assumption of heterostructure theory is the "electron affinity rule": that is, the conduction band discontinuity is simply the difference between the electron affinity of the two materials,

$$\Delta\varepsilon_c = \chi_1 - \chi_2 \ , \tag{2}$$

presumably referenced to the infinite vacuum level.

4.1 CURRENT PROBLEMS

Kroemer [7] has pointed out a number of problems with this concept, the most important of which are: (1) assuming the rule is valid, the band discontinuities need to be known to an accuracy of about a kT, while the affinities, usually referenced to a near vacuum level, cannot be measured that accurately; (2) the basic differences between free surfaces and solid interfaces are so great that there

is no fundamental reason for expecting any relationship between electron affinities and band discontinuities. Thus, to resolve this problem, it is necessary to forget about phenomenological surface properties and look at the interface problem from a microscopic point-of-view.

In spite of these arguments, Shay *et al* [8] compared measured band discontinuities for several heterojunctions with measured electron affinities from photoemission data and calculated affinities from the dielectric two-band model. They found that the agreement between the measured discontinuities and those calculated from the affinity rule was very good. In addition, Frensley and Kroemer [9] found from a pseudopotential calculation of a heterojunction interface that the affinity rule is approximately correct. Although this is a somewhat surprising result, Kroemer's original objections are, of course, still valid.

More recently, Adams and Nussbaum [10] have examined the affinity rule from an electrostatic point-of-view. They suggest that instead of keeping the vacuum level continuous (the electron affinity rule) it may be more appropriate to assume continuity of the intrinsic level. This paper is interesting because it also, although unintentionally, demonstrates another problem with heterojunction theory: the usual equilibrium and non-equilibrium formulations in the depletion approximation are not self-consistent. This inconsistency occurs regardless of which basic assumption is used.

The problem arises in the following manner: For simplicity assume an abrupt p-n heterojunction. In equilibrium, the built-in potential of the space-charge region is given by,

$$V_0 = \frac{kT}{q} \ln\left(\frac{N_d N_a}{n_{in} n_{ip}}\right), \tag{3}$$

where N_d and N_a are the donor and acceptor concentrations on the n and p side of the heterojunction, respectively, and n_{in} and n_{ip} are the intrinsic concentrations. When the heterojunction is forward-biased with a voltage V, in the depletion approximation the holes injected into the n-side at the edge of the depletion region is usually found to be,

$$p_n = p_p \exp\left[\frac{q(V-V_0)}{kT}\right] . \tag{4}$$

If V is turned off, the excess holes disappear and

$$p_n = \frac{n_{in}^2}{N_d} \quad , \quad p_p = N_a ,$$

and

$$V_0 = \frac{kT}{q} \ln\left(\frac{N_d N_a}{n_{in}^2}\right) . \tag{5}$$

Comparing Eqs. (3) and (5), we see that this analysis is only valid for a p-n homojunction.

The problem we wish to consider is the latter one, although the electron affinity rule is a natural consequence of our analysis. We will show that the inconsistency arises from the neglect of a thermodynamic force term, which is well understood but, apparently, not widely known.

4.2 THERMODYNAMIC ANALYSIS

For any solid it can be shown [11] that the entropy source strength (entropy production rate per unit volume) is,

$$\sigma_s = \vec{J}_Q \cdot \vec{\nabla}\left(\frac{1}{T}\right) + \sum_i \vec{j}_i \cdot \left[\frac{\vec{F}_i}{T} - \vec{\nabla}\left(\frac{\mu_i}{T}\right)\right] + \sum_j \frac{A_j}{T} v_j \geq 0. \qquad (6)$$

In this equation $\vec{J}_Q$ is the heat flux (flux of internal energy), $\vec{j}_i$ are the particle fluxes for each i component, $\vec{F}_i$ are the forces, μ_i are the chemical potentials, A_j are the chemical affinities of the j quasi-chemical reactions, and v_j are the reaction rates. From the second law of thermodynamics, the entropy source strength is positive definite and equal to zero in equilibrium.

The basic assumption underlying this model is the concept of "local equilibrium". That is, although the whole system may be far from equilibrium, the particles in each differential volume are in equilibrium with each other. If one considers the small distances and interaction times among particles within a differential volume and the large distances and interaction times among particles from different differential volumes of a system, the concept of local equilibrium is a reasonable one.

For our purposes here we neglect any temperature gradients or quasi-chemical reactions and assume that the only force on the particles is an electrostatic potential gradient. Equation (6) then reduces to,

$$\sigma_s = -\frac{1}{T}\sum_i \vec{j}_i \cdot \vec{\nabla}\zeta_i \geq 0, \tag{7}$$

where ζ_i is the electrochemical potential. Consider the form of σ_s near equilibrium by expanding it in a series of the generalized forces around $\vec{\nabla}\zeta_i = 0$. The first term is zero because $\sigma_s = 0$ in equilibrium, and the second term, linear in $\vec{\nabla}\zeta_i$, is zero because σ_s is positive definite. The third term, quadratic in $\vec{\nabla}\zeta_i$, is the first non-zero term. Retaining only this term we can see that, to first order, near equilibrium,

$$\vec{j}_i \alpha - \vec{\nabla}\zeta_i \ . \tag{8}$$

Going from particle current to electric current, Eq. (8) tells us that the correct expression for the equation-of-state of this isothermal system is,

$$\vec{J}_i = n_i \mu_i \vec{\nabla}\zeta_i \ , \tag{9}$$

where n_i and μ_i are the concentration and mobility of the i particles. Equation (9), of course, is a well-known result. We went through this analysis to show that it is correct to first order, under the assumptions discussed, and that it can be derived from the second law of thermodynamics. In general, all of the quantities in Eq. (9) can vary with position and time.

We now need to obtain an expression for the electrochemical potential for indistinguishable particles. For a

grand canonical ensemble of particles near equilibrium, it can be shown [12] that the distribution function is approximately,

$$f = \left[1 + \exp\left(\frac{\varepsilon-\zeta}{kT}\right)\right]^{-1} \tag{10}$$

That is, it has the same form as the Fermi-Dirac distribution except that, in general, f, ε, ζ, and T can vary in time and position. Equation (10) is obtained under the local equilibrium assumption and is valid only to first order. Thus, Eqs. (9) and (10) are derived with the same assumptions and approximations, and we can use them to analyze heterostructures keeping this in mind.

4.3 HETOROJUNCTION MODEL

Let us apply Eq. (10) to obtain an expression between the concentration of electrons in the conduction band and their electrochemical potential. In the usual way, we multiply the distribution function times the density-of-states and integrate over the band to obtain,

$$n = \int_{\varepsilon_c}^{\infty} g(\varepsilon) f(\varepsilon) d\varepsilon \ , \tag{11}$$

where ε_c is the bottom of the conduction band. For a dilute distribution of electrons, Eq. (11) gives,

$$n = N_c \exp\ (\zeta - \varepsilon_c), \tag{12}$$

where N_c is the effective density-of-states of the conduction band. In general, all four quantities in Eq. (12) can vary with time and position.

Using Eqs. (9) and (12), we have the general near-equilibrium equation-of-state for electron flow in a heterojunction,

$$\vec{J}_n = n\mu_n \vec{\nabla}\left(\varepsilon_c + kT \ln \frac{n}{N_c}\right) \quad (13)$$

Notice, that all of the quantities in this equation can, in general, vary with position and time including N_c. It is the neglect of the term $-\vec{\nabla}(\ln N_c)$ which leads to the inconsistency mentioned previously. A similar expression can be obtained for the hole current:

$$\vec{J}_p = p\mu_p \vec{\nabla}\left(\varepsilon_v - kT \ln \frac{p}{N_v}\right) . \quad (14)$$

Let's examine each of the thermodynamic forces in Eqs. (13) and (14). The forces $\vec{\nabla}\varepsilon_c$ and $\vec{\nabla}\varepsilon_v$ represent variation in composition or bandgap as well as applied and built-in electric fields due to space charge. The component of these forces which has equal and opposite effect on electrons and holes can be associated with electric field, with the rest associated with band-gap variations. The forces $\vec{\nabla}(\ln n)$ and $-\vec{\nabla}(\ln p)$ are the usual diffusion terms. The thermodynamic forces $-\vec{\nabla}(\ln N_c)$ and $\vec{\nabla}(\ln N_v)$ can be regarded as entropy forces: that is, they act to drive the electrons and holes to regions of higher density-of-state or higher entropy. These forces are required, therefore, by the second law of thermodynamics, and must be included in a heterostructure analysis.

We will now show that including these entropy forces eliminates the inconsistancy in the analysis of an abrupt p-n heterojunction. In equilibrium, from Eqs. (13) and (14) the built in potential of the space charge region is,

$$qV_0 = \Delta\varepsilon_c + kT\ln\left(\frac{n_n N_{cp}}{N_{cn} n_p}\right) , \tag{15}$$

or

$$qV_0 = -\Delta\varepsilon_v + kT\ln\left(\frac{p_p N_{vn}}{N_{vp} P_n}\right) . \tag{16}$$

Using Eq. (1) these two expressions can be shown to be equal. When the junction is forward-biased, the holes injected into the n-side in the depletion approximation are,

$$P_n = P_p \frac{N_{vn}}{N_{vp}} \exp\left[\frac{q(V-V_0)-\Delta\varepsilon_v}{kT}\right] . \tag{17}$$

Turning the applied voltage off in Eq. (17), we obtain Eq. (16) and the inconsistancy is removed.

Notice that in this analysis we have made no assumptions about the continuity of the infinite vacuum level (electron affinity rule) or any other level. However, if we refer to Eqs. (7) and (8), in equilibrium there is no entropy production and

$$\sum(\vec{\nabla}\zeta_i)^2 = 0 , \tag{18}$$

or

$$\vec{\nabla}\zeta_i = 0 . \tag{19}$$

If the electrochemical potentials are referenced to the infinite vacuum level, then it must be continuous.

5. INERTIAL TRANSPORT IN NONPARABOLIC BANDS

Since the primitive unit cell of the II-IV-V_2 chalcopyrites is four times as large as that of their III-V sphalerite analogs, the first Brillouin zone is one-fourth as large. For this reason and because of their small effective masses, a potential application for these chalcopyrites may be in inertial transport devices (if such devices can be realized).

The reprint in this section shows what current-voltage characteristics a space-charge limited diode would have if the charge carriers are not scattered in a nonparabolic band.

Collisionless Space-Charge Limited Currents in Semiconductors with Nonparabolic Bands

M. W. MULLER

Abstract—The current-voltage relation for space-charge limited collisionless flow is computed for a model semiconductor with a hyperbolic band structure as deduced from two-band $\bar{k} \cdot \bar{p}$ perturbation theory. The expected current is reduced significantly below the constant effective mass value for voltages in excess of the bandgap, and the high-voltage asymptotic relation is V rather than $V^{3/2}$.

Manuscript received October 27, 1980; revised December 5, 1980. This work was supported by ONR Contract N00014-79-C-0840 and AFOSR Contract 79-0096.

The author is with the Department of Electrical Engineering, Washington University, St. Louis, MO 63130.

In devices that use high-mobility, low effective mass semiconductors, the mean free time between collisions of a carrier can become equal to, or longer than an oscillation period, or the mean free path between collisions equal to or longer than a typical device dimension.

Under such conditions the carrier transport in semiconductors is not governed by the traditional friction-dominated Ohm's law behavior. The motion of the carriers for the short times or distances of primary interest for device operation may be more accurately described by the inertial or ballistic equation of motion.

The simplest device for studying inertial transport is the short space-charge limited semiconductor diode. Calculations of the behavior of such diodes, without collisions, and with few collisions [1] have been reported. These calculations assume that the carrier effective mass is independent of energy.

In a device that operates in a collision-free, or nearly collision-free regime, the carriers that contribute to the device current reach energies corresponding to the voltages applied to the device. In small and fast devices, these are of the order of 1 V. In most semiconductors, especially those with small effective mass carriers, the bands depart from parabolicity at energies well below 1 eV. The effective mass generally increases with energy. Thus the current is smaller than one would predict for a parabolic band structure.

To assess the magnitude of this effect, we use the conduction band structure of a model narrow-gap semiconductor as computed by two-band $\bar{k} \cdot \bar{p}$ perturbation theory. Such a model can provide a fair approximation to the real band structure in the vicinity of the conduction band extremum.

Assuming a direct-gap semiconductor, and placing the zero of energy at the conduction band minimum, the theory gives the hyperbolic band structure

$$\epsilon = \frac{1}{2}\epsilon_g\left[\sqrt{1+\frac{2\hbar^2k^2}{m^*\epsilon_g}}-1\right]. \tag{1}$$

The theory also provides a relation between the effective mass m^* and the bandgap ϵ_g, but for the present purpose these two parameters may be chosen independently, for instance to fit a measured band structure.

To obtain the carrier velocity as a function of energy, we use

$$\frac{\partial\epsilon}{\partial k} = \frac{\hbar^2 k}{m^*}\left(1+\frac{2\hbar^2k^2}{m^*\epsilon_g}\right)^{-1/2} \tag{2}$$

and then solve (1) for k^2

$$k^2 = \frac{2m^*}{\hbar^2}\left(\epsilon+\frac{\epsilon^2}{\epsilon_g}\right). \tag{3}$$

Substituting this in (2) gives

$$\frac{\partial\epsilon}{\partial k} = \sqrt{\frac{2}{m^*}}\frac{\hbar(\epsilon+\epsilon^2/\epsilon_g)^{1/2}}{1+\epsilon/\epsilon_g} = 2\hbar v_s\frac{\epsilon/\epsilon_g+\epsilon^2/\epsilon_g^2}{1+2\epsilon/\epsilon_g}$$

$$= \hbar v_s\frac{(2m^*v_s^2\epsilon+\epsilon^2)}{m^*v_s^2+\epsilon} \tag{4}$$

0018-9383/81/0500-0604$00.75

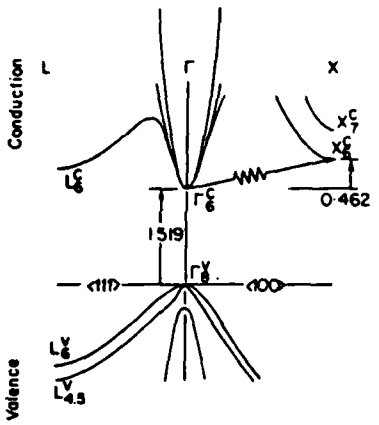

Fig. 1. GaAs band structure with parabolic and hyperbolic conduction band approximation.

where we have defined a band-structure limited velocity

$$v_s \equiv (\epsilon_g/2m^*)^{1/2}. \tag{5}$$

Fig. 1 shows the current best plot of the GaAs band structure [2] with both (1) using the experimental ϵ_g and m^*, and a $\hbar^2k^2/2m^*$ parabola superposed on the plot. The hyperbola of (1) is evidently a much better fit.

The Poisson equation for a semiconductor uniformly doped with n_0 donors/cm^3 carrying an electron current density J is

$$\frac{d^2V}{dx^2} = \frac{\rho}{\epsilon} = -\frac{qn_0}{\epsilon} + \frac{J}{\epsilon v} \tag{6}$$

where ϵ is the dielectric constant and v is the electron velocity.

Electrons injected at $x = 0$ acquire a velocity

$$v = \frac{1}{\hbar}\frac{\partial \epsilon}{\partial k} \tag{7}$$

when their energy $\epsilon = qV \equiv \phi$.

Using the band structure gradient from (4) brings the Poisson equation into the form

$$\phi'' = -\frac{q^2n_0}{\epsilon} + \frac{Jq}{\epsilon v_s}\frac{(m^*v_s^2 + \phi)}{(2m^*v_s^2\phi + \phi^2)^{1/2}} \tag{8}$$

where a prime denotes d/dx. Equation (8) can be integrated once to give

$$(\phi')^2 - (\phi'(0))^2 = \frac{2Jq}{\epsilon v_s}(\phi^2 + 2m^*v_s^2\phi)^{1/2} - \frac{2q^3n_0}{\epsilon}\phi. \tag{9}$$

Assuming space charge limitation $\phi'(0) = 0$, and changing to reduced variables

$$u \equiv \frac{\phi}{2m^*v_s^2}, \quad j = \frac{J}{qn_0v_s}, \quad \lambda = \frac{x}{(\epsilon m^*/n_0q^2)^{1/2}v_s} \tag{10}$$

we can write the diode equation, the integral of (9), in the form

$$\int_0^u du\,[j(u^2 + u)^{1/2} - u]^{-1/2} = l$$

where $u = v(V = V_0$, the applied voltage) at $\lambda = l(x = L$, the diode length). The normalized variables are: diode voltage in units of $2m^*v_s^2/q$—four times the kinetic energy the carriers would have if their effective mass were constant at the band edge value, and they were moving with the limiting velocity v_s; if the $\vec{k}\cdot\vec{p}$ perturbation theory is taken literally, this unit is equal to ϵ_g/q; current density in units of qn_0v_s—the current that would flow if the mobile carriers from the doping were moving with velocity v_s; diode length in units of $v_s\tau_p$, with τ_p the plasma oscillation period of the semiconductor.

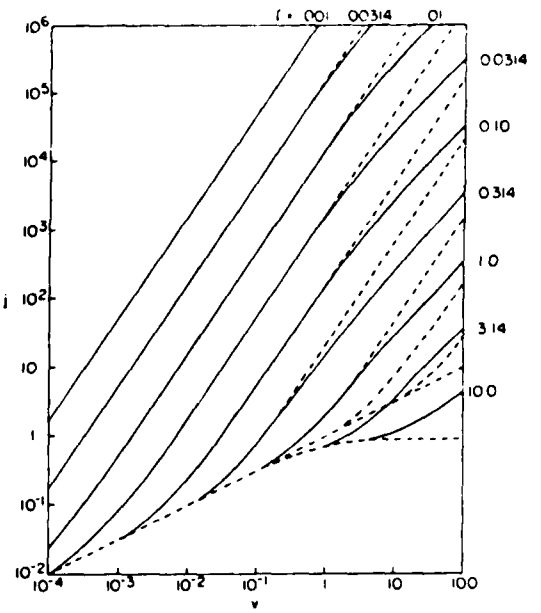

Fig. 2. Space-charge limited current-voltage relation of a collisionless semiconductor.

Curves of current density versus voltage are shown in Fig. 2 as full curves. For comparison the current density-voltage curves one would compute assuming constant effective mass are shown dashed.

The vacuum diode analog 3/2 power law holds only for $V_0 \lesssim \epsilon_g$, and then only for $l \lesssim 1$. That means very short diodes—for GaAs with $n_0 = 10^{16}$, shorter than 0.25 μm. The limiting higher voltage behavior is $J \propto V$ rather than $J \propto V^{3/2}$; the J–V curves bend over.

In the typical size and operating voltage range of GaAs devices the corrections indicated here appear significant but not dramatic. They are likely to be rather more important in devices made from smaller bandgap, lower m^* material.

We have not extended the diode characteristics into the low-current region at the lower ends of the curves. The problems encountered by modeling this operating regime are rather complicated, involving multiple-valued functions and possibly spatial and temporal instabilities [3]. Moreover, the neglect of collisions and thermal energies is less justifiable in this low-voltage region.

References

[1] M. S. Shur and L. F. Eastman, *IEEE Trans. Electron Devices*, vol. ED-26, p. 1677, 1979; and *IEEE Electron Device Lett.*, vol. EDL-1, p. 147, 1980.

[2] D. E. Aspnes, in *Proc. 6th Internat. Symp., GaAs and Related Compounds*, L. F. Eastman, Ed. London: Inst. Phys., 1977.

[3] B. Abraham-Shrauner, in Rep. ONR 80-1, Washington Univ., unpublished.

6. REFERENCES

1. V.V. Podoliskiy, I.A. Karpovich, and B.N. Zvonkov, "Hall Mobility of Electrons in $CdSnP_2$ Single Crystals", *Soviet Physics of Semiconductors* 10, No. 5, 594, (1976).

2. J.L. Shay and J.H. Wernick, *Ternary Chalcopyrite Semiconductors: Growth, Electronic Properties, and Applications*, Pergamon Press, Elmsford, New York, (1975).

3. J.L. Shay, K.L. Bachman, and E. Buehler, "Preparation and Properties of $CdSnP_2$/InP Heterojunctions Grown by LPE from Sn Solution", *Journal of Applied Physics* 45, No. 3, 1302, (1974).

4. G.A. Davis, "Liquid Phase Epitaxial Growth of $Zn_xCd_{1-x}SnP_2$", Master's Thesis, Washington University, Unpublished.

5. Albert C. Beer, *Galvanomagnetic Effects in Semiconductors*, Academic Press, New York, New York, (1963).

6. C.M. Wolfe, G.E. Stillman, and J.A. Rossi, "High Apparent Mobility in Inhomogeneous Semiconductors", *Journal of the Electrochemical Society* 119, No. 2, 250, (1972).

7. H. Kroemer, "Problems in the Theory of Heterojunction Discontinuities", *Critical Reviews of Solid State Science* 5, 555, (1975).

8. J.L. Shay, S. Wagner, and J.C. Phillips, "Heterojunction Band Discontinuities", *Applied Physics Letters* 28, 31, (1976).

9. H.R. Frensley and H. Kroemer, "Prediction of Semiconductor Heterojunction Discontinuities from Bulk Band Structures", *Journal of Vacuum Science and Technology* 13, 810, (1976).

10. M.J. Adams and A. Nussbaum, "A Proposal for a New Approach to Heterojunction Theory", *Solid-State Electronics* 22, 783, (1979).

11. P. Glansdorff and I. Prigogine, *Thermodynamic Theory of Structure, Stability, and Fluctuations*, (Wiley-Interscience, London, 1971).

12. D.N. Zubarev, *Nonequilibrium Statistical Thermodynamics*, (Consultants Bureau, New York, 1974).

7. PUBLICATIONS

1. M.W. Muller, "Collisionless Space-Charge Limited Currents in Semiconductors with Nonparabolic Bands", IEEE Transactions on Electron Devices 28, 604, (1981).

2. G.A. Davis and C.M. Wolfe, "Liquid Phase Epitaxial Growth of Zn_xSnP_2", to be submitted to Journal of Electronic Materials.

8. PERSONNEL

The personnel who worked on this grant during the current reporting period were:

Prof. C.M. Wolfe, Principal Investigator

Prof. M.W. Muller, Faculty Associate

Mr. Gary A. Davis, Graduate Research Assistant

Ms. S. Julie Hsieh, Graduate Research Assistant

Mr. Davis has completed the requirements for the master's degree in electrical engineering and Ms. Hsieh has a master's degree in physics. Both are doctoral candidates.

The degrees awarded on this grant up to the present time are:

August 1980, Camellia M.L. Yee, Master of Science, Chemical Reactions in the Vapor Phase Growth of $ZnGeAs_2$.

9. MEETING TALKS

1. Camellia M.L. Yee, Heidi J. Carroll, and C.M. Wolfe, "Chemical Vapor Deposition of $ZnGeAs_2$ on GaAs", Electronic Materials Conference, Ithaca, NY, 24-27 June 1980.

2. G.A. Davis and C.M. Wolfe, "Liquid Phase Epitaxial Growth of $CdSnP_2$", Electronic Materials Conference, Ithaca, NY, 24-27 June 1980.

3. M.W. Muller, "Inertial Transport with Non-Parabolic Bands", Late News Paper, International Symposium on GaAs, Vienna, Austria, 22-24 September 1980.

4. C.M. Wolfe, "Amphoteric Dopants and Compensation in GaAs", Workshop on Shallow Impurities in Semiconductors, Wright-Patterson AFB, Ohio, 21-22 May 1981.

5. G.A. Davis and C.M. Wolfe, "Liquid Phase Epitaxial Growth of $Zn_xCd_{1-x}SnP_2$", Electronic Materials Conference, Santa Barbara, California, 24-26 June 1981.


DA
FIL